Synthesis and deposition of silver nanoparticles on porous titanium substrates for biomedical applications

Juliana Gaviria[1], Ana Alcudia[2], Belén Begines[2], Ana María Beltrán[3,*], Junes Villarraga[1], Rocío Moriche[3], José Antonio Rodríguez-Ortiz[3] and Yadir Torres[3]

[1] Grupo de Biomateriales Avanzados y Medicina Regenerativa, BAMR. Facultad de Ingeniería Universidad de Antioquia, Medellín, Colombia

[2] Departamento de Química Orgánica y Farmacéutica, Facultad de Farmacia, Universidad de Sevilla, Seville, Spain

[3]Departamento de Ingeniería y Ciencia de los Materiales y del Transporte, Escuela Politécnica Superior, Universidad de Sevilla, Seville, Spain.

*** Corresponding author:**

Ana M. Beltrán, PhD

Departamento de Ingeniería y Ciencia de los Materiales y del Transporte

Escuela Politécnica Superior, Universidad de Sevilla

Virgen de África 7

41011 Sevilla, Spain

Email: abeltran3@us.es

Phone: +34954550131

Fax: +34 954460475

Abstract

Ti implants are highly biocompatible and allow orderly bone growth but, unfortunately, in the first five years after implantation, 5–10 % of them fail due to poor osseointegration and to the presence of bacterial infections in prosthesis. Silver nanoparticles have been described to damage bacterial cell via prolonged release of Ag^+ ions as a mode of action when immobilized on a surface. In this work, two routes to synthetize silver nanoparticles have been proposed including, on the one hand, a $NaBH_4$-reduction and, on the other hand, a citrate-reduction combined with a stabilized biodegradable polymer. The

deposition of these nanomaterials on porous Ti substrates previously fabricated using the space-holder technique (40 vol.% and two size distributions, 100–200 and 355–500 μm) was investigated to aim for the best match. Before the deposition of nanoparticles accomplished by immersion, a silanization treatment of the substrate surface was carried out. After silver nanoparticles were deposited on the porous Ti substrates, microstructural characteristics and antibacterial behavior were evaluated against the proliferation of *Staphylococcus aureus* on the AgNPs functionalized substrates. Finally, the preliminary qualitative analysis showed the presence of inhibitory halos, being more relevant in the substrates with larger pores.

Keywords: porous titanium; silver nanoparticles synthesis; biofunctionalized surface; antibacterial behavior.

1. Introduction

Prostheses have been used to replace bones or missing teeth since antiquity as it was mentioned in the Pindar´s First Olympian Ode (522-433 BCE). They are designed for functional or aesthetics reasons as an artificial extension to fulfill the performance of the missing body part [1]. The current prosthetic solution contributes to overcome the limitations and to promote the capability of performing daily living, working or social activities. Hence, the sophistication and variety has dramatically increased in the last decades to aid in restoring the structure or function of the musculoskeletal system and to enhance the quality as well as longevity of human life [2]. Also, the areas related to this field have led to create an increasing multi-million-dollar business that will probably continue rising.

The field of biomaterials focused on prosthesis has become a crucial area. Among the materials used for these purposes are ceramics, polymers, composites and, specially, the Ti-based alloys. As it is well known, Ti prosthesis are costlier but, on the other hand, they possess better biological compatibility, mechanical performance and superior corrosion resistance that, in summary, brings out their clear superiority [3–5]. In this sense, the micro and nano-scale superficial modification reveals beneficial effects in terms of biocompatibility

since it allows bone growth towards the implant while maintaining the mechanical requirements of cortical bone tissues [6,7]. Otherwise, the adequate texturing methodologies entails surface modification techniques to achieve superior biocompatibility, higher wear and corrosion resistance. However, a field to explore remains, given their prohibitive costs and lack of clinical validation in most cases. In general, Ti implants are highly biocompatible and allow orderly bone growth, but unfortunately, in the first five years after implantation, 5–10 % fails due to poor osseointegration. Biomechanical malfunction may favor bacterial infections, also known as a catastrophic complication [8] which is associated with additional costs, estimated to be around 100,000 USD per patient [9]. Indeed, several prophylactic measures are becoming usual to prevent severe infections, such as using aseptic techniques or intake of antibiotics preoperatively, but it is not the panacea and still the incidence remains quite high.

At this point, there is an urgent demand for developing powerful strategies to minimize the risk of implant-related infections and its life-threatening complications. In the literature, two approaches for preventing infections have been investigated: (a) fabricating implants with materials containing intrinsic antibacterial properties, like Ag, Cu, Zn or the biopolymer chitosan, obtained from the deacetylation of chitin, a natural biopolymer [10]; and (b) via functionalization of the implant surface (through modification of surface chemistry or morphology, or applying a coating) [11]. In this context, it is crucial to act from the early phase of infection (it does not mean just after the surgery, but when initial steps are begun before a severe infection is spreading). In the early stages, bacterial adhesion to surface takes part before proliferation [12], subsequent biofilm formation and successive invasion of other tissues occurred via diffusion [13]. In this context, due to the slow approval rate for new antibiotics as well as the resistance problems associated to bacterial infections, there is an enormous demand for new potent biocides to act as effective coatings in prosthesis.

Interestingly, nanotechnology is emerging as a new interdisciplinary field combining biology, physics, chemistry, engineering, and material science and offering new and practical

solutions in different areas related to medicine or pharmacy, from a divergent and more innovative point of view [14,15]. Nanoparticles (NPs) are particles of matter within the range of nanometers in diameter, with a high surface to volume ratio, good stability in general and facile surface modification [16]. All these characteristics confer them exceptional and potent antibacterial behavior as well as low toxicity towards mammalian cells. Furthermore, metallic nanoparticles, especially silver nanoparticles (AgNPs), have been described to damage bacterial cell via prolonged release of Ag^+ ions as a mode of action when immobilized on the surface. They have been widely employed in medicine taking advantage of their broad and high antimicrobial activity and low cytotoxity, tested using cell viability studies [4,17]. In this sense, there are numerous publications in the literature regarding the goodness of the antibacterial activity of Ti functionalized with AgNPs [18–20]. On the other hand, metallic nanoparticles stabilized using organic moieties, such as polymers, is a recent route developed to further extend the antimicrobial applications of metals [21]. The incorporation of metallic NPs into polymer matrices could be considered as novel polymer/metal composites materials which could lead to new and interesting entities to investigate in which the organic portion could enhanced ADME properties (absorption, distribution, metabolism and excretion) taking advantage of the potential polymer degradation [22].

The aim of this study is to explore, on the one hand, two different Ti substrates, porous and fully-dense, obtained by space-holder technique and conventional powder technology, respectively. On the other hand, to prevent infections, a silver NPs coating was considered, taking advantage of their bactericidal effect, selecting from two different NPs synthesis routes, to optimize the biomechanical and biofunctional behavior.

2. Materials and Methods

Figure 1 summarizes the workflow of this investigation, from the fabrication of the substrates, two routes employed for the synthesis of the AgNPs as well as the characterization of the coated substrates.

2.1. Fabrication and characterization of the porous titanium substrates.

Two types of substrates were studied in this work, both of them from commercially pure titanium (c.p. Ti) powder, grade IV (according to ASTM: F67-13), with a mean particle size of $d_{[50]}$ = 23.3 μm [23], provided by SEJONG Materials Co. Ltd. (Seoul, Korea). On the one hand, fully-dense substrates were fabricated by conventional powder metallurgy technique (PM), pressing at 1300 MPa using an Instron 5505 universal testing machine (Instron, U.K.) and, then, sintering (1300 °C for 2 h, and high vacuum condition, 10^{-5} mbar) in a ceramic tubular furnace. Porous substrates were manufactured by space-holder technique (SH), mixing c.p. Ti powder and 40 vol.% of ammonium bicarbonate (NH_4HCO_3), (BA), with a purity of 99 %, supplied by Cymit Química S.L. (Spain), as spacer particles of two ranges in size (100–200 μm and 355–500 μm). Once the blend was homogeneous, it was pressed with the same equipment at 800 MPa. Then, the BA was removed in an oven at 10^{-2} mbar, firstly at 60 °C for 12 h and secondly at 110 °C for 12 h. After that, the green compacts were sintered for 2 h at 1250 °C and 10^{-5} mbar in a ceramic tubular furnace.

Image analysis and Archimedes' method was used to evaluate the equivalent pore diameter, as well as the total and interconnected porosity (D_{eq}, P_T, and P_i, respectively) [24], in order to corroborate the reliability of the manufacturing route. While, the mechanical behavior of the porous substrates (dynamic Young´s modulus, E_d, yield strength, σ_y), were estimated using the equations reported in the literature [25].

2.2. Synthesis and characterization of the AgNPs.

Two different methodologies were tested in parallel for the synthesis of the AgNPs: route A and route B (polymer-protected AgNPs). The first methodology, proposed by Lee & Melsel [26], consisted of dissolving $AgNO_3$ (2 mM) in deionized water. Under a continuous stirring at 115 rpm and 0 °C, $NaBH_4$ (1 vol. %) was added and the mixture was left reacting for 30 min [27,28]. A yellowish suspension of AgNPs was obtained. The second methodology was

based on the preparation of an AgNP-polymer nanocomposite. The polymer matrix used as stabilizer of the AgNPs was a copolyurethane composed by arabinitol (sugar)-, dithiodiethanol-, and 1,8-octanediol- based units in a molecular ratio of 25, 25 and 50 %, respectively (Figure 2) [29]. These three different units were obtained from the polyaddition reaction between hexamethylene diisocyanate (HDI) and the corresponding diol to generate the urethane bonding. The chemicals and solvents were purchased from Aldrich Chemicals Co and were used without further purification. The original method followed to synthesize this copolyurethane was developed and previously reported by the authors [29]. Once synthesized, it was dissolved in dry dimethyl sulfoxide (DMSO) under vigorous magnetic stirring agitation, using a concentration of 10 mg/ml [30].

For the route B, the process used to synthesize AgNPs was based on a previously reported method proposed by N. G. Bastús et al. [31]. In it, $AgNO_3$, trisodium citrate (SC) and tannic acid (TA), purchased from Sigma-Aldrich, were utilized as precursors without further purification. $AgNO_3$ was dissolved in DMSO (25 mM) while aqueous solutions of SC (1.1 M) and TA (0,012 mM) were also prepared. Molarities were adjusted to minimize H_2O content since excessive amounts could cause the precipitation of the copolyurethane. Initially, solutions containing the $AgNO_3$ and the copolyurethane were mixed under vigorous magnetic stirring agitation at 80 °C. The $AgNO_3$/copolyurethane ratios were set to achieve concentrations of AgNPs of 0.1, 0.2, and 0.4 wt. % in resulting nanocomposites. Once mixing was complete, SC and TA solutions were added sequentially in needed quantities, depending on AgNPs wt. %, to achieve SC/$AgNO_3$ and TA/$AgNO_3$ molar ratios of 20 and 0.1, respectively. Stabilization of the solution yellowish color was observed after 10 minutes.

After preparation of nanocomposites, UV-Vis absorbance spectroscopy was used to corroborate the presence of AgNPs. Measurements were carried out in an Agilent *Cary 5000* spectrophotometer at 298 K from 300 up to 600 nm with a wavelength accuracy of ± 0.3 nm and a spectral bandwidth of 0.5 mm. In order to check the quality (size distribution,

composition) of the Ag nanoparticles, they were characterized by transmission and scanning-transmission electron microscope techniques (TEM and STEM, respectively) using a FEI TALOS 200 kV microscope and an FEI Tecnai G2 F20 (both microscopes by FEI, Eindhoven, The Netherlands). They were equipped with Super-X energy dispersive X-ray spectrometry (EDX) system which includes two silicon drift detectors for compositional analysis. For TEM studies, a drop of the solution was deposited on an ultra-thin carbon film on a nickel grid.

2.3. Deposition, micro-structural and anti-bacterial characterization of the deposited AgNPs

Deposition of AgNPs on the surface of the fully-dense and porous c.p. Ti substrates, which were previously grinded and polished, consisted of three stages: hydroxylation of Ti substrates, surface silanitazion and submersion in the AgNPs suspension.

Fully-dense and porous c.p. Ti samples were immerse in acid solution at 60 °C for 24 h. Acid solution, also known as piranha solution, was prepared as a mixture 3:7 of H_2O_2 (30 vol. %) and H_2SO_4 (70 vol. %). Substrates were later washed three times with water and dried with a N_2 flow. Hydroxylated samples were treated with a solution of 3-aminopropyltrietoxysilane (APTES) (1 vol. %) in water for 15 min under continuous stirring and dried in an oven equipped with convective air flow at 115 °C for 1.5 h. Additionally, they were again washed three times with water and dried with a N_2 flow. Finally, AgNPs deposition to the substrate surfaces was achieved by their submersion in the prepared nanoparticle suspension for 30 min.

Once the fully-dense and/or porous substrates were coated by the Ag nanoparticles, they were characterized by scanning electron microscopy (SEM) using a JEOL scanning electron microscope, model JSM 6490-LV. Compositional analyses were performed by energy dispersive spectroscopy (EDS) coupled to the scanning electron microscope (EDS-SEM).

The antibacterial capability of the coated Ti substrates was evaluated by the Kirby-Bauver diffusion method using Staphylococcus aureus (ATCC 25923). Plates containing

Müller-Hinton medium were streaked with a bacteria-enriched TSA suspension utilizing sterile swaps. The substrates with and without AgNPs were placed face down onto the medium surface and plates were cultured at 37 °C for 24 h in aerobic conditions. Growth inhibition zone formation was identified around the titanium sample, photographically recording the formation of inhibition halos, which were measured using ImageJ program. For statistical analysis, three measurements were taken in each of the three samples (n = 3) of the different titanium discs and control. So, in total, 18 readings were performed, which correspond to the 3 measurement of the 3 discs for the two different samples, the uncoated for reference and the AgNPs-coated substrates.

3. Results and Discussion

Firstly, in this work, substrates were characterized after their fabrication to evaluate the porosity (percentage, morphology and size of the pores) as well as estimate the mechanical properties. Then, the synthesis of the AgNPs was described in detail for both routes as well as their characterization from which the best one would be selected. Next, the substrates coated with the AgNPs were analyzed. Finally, the antibacterial behavior of the coated samples was evaluated.

3.1. Characterization of the c.p. Ti uncoated substrates.

Table 1 summarizes the microstructural and mechanical characterization of the uncoated titanium substrates. The analysis of these results indicates that: 1) the content and size of the spacer particles used allows the control of total porosity and the size of the pores obtained, corroborating the reliability of the manufacturing route, 2) higher values of interconnected porosity were obtained when using smaller spacer particles due to the higher probability of coalescence of the pores, and 3) the estimated yield strength is consistent with the equivalent diameter of the pores.

3.2 Synthesis and characterization of AgNPs

In our search for the best coating to cover these metallic samples, two approaches based on AgNPs were developed. In the first one, ice-cold sodium borohydride was addeed dropwise to reduce not only the ionic silver but also to stabilized the already formed nanoparticles. Just after this addition, a grey suspension which involves a quick nucleation and a temporary aggregation was formed, and after a few seconds under vigorous stirring to dissolve the $NaBH_4$ at 0 *°C*, the crude reaction turned to pale yellow avoiding non-convenient nanoparticle aggregation [32]. Controlling the temperature during the synthesis is a crucial issue to avoid the undesirable formation of extra subproducts consequent of the potent reductor effect of the $NaBH_4$.

AgNPs were generated in the presence of a biocompatible, biodegradable and synthetic comb-like polymer prepared following the methodology developed in our group from a renewable and cheap source like arabinitol sugar [29,30]. It has been previously described in the literature that using appropriated polymers in combination with metal nano-structures (Figure 3) leads to an unique system in which not only nanoparticles stability was enhanced and aggregation prevented, but also the hydrophilic/hydrophobic interactions could lead to a high level of packing, conferring attractive properties from a biomedical point of view.

In particular, the polymer was based on three different units which were obtained from hexamethylene diisocyanate (HDI) and a diol to generate the urethane bonding. The mixture of the units in different proportions and a subsequent Click Chemistry reaction with methoxypolyethylene glycol azide led to the different types of copolyurethanes. For this copolyurethane, a 25 % of the sugar-based unit was used together with a 25 % of the dithiodiethanol-derived one plus a 50 % of the octanediol-based fraction (Figure 2).

The use of polymeric materials as nanoparticle stabilizers has been previously described in the literature [33,34]. The most important characteristic of polymeric stabilizers is the increment of stability they produce in the nanoparticulate system [30,35,36]. However, they

may produce unpredictable behavior when compared with $NaBH_4$-reduced nanoparticles or stabilized with low molecular weight materials. Therefore, to estimate how silver concentration affects to the nanoparticle formation and stability, 3 different Ag/copolyurethane composites were prepared including 0.1, 0.2, and 0.4 Ag/copolyurethane wt. % in the final material.

For AgNPs characterization, initial UV-Vis studies were conducted. Silver nanoparticles show surface plasmon resonance due to coherent fluctuations which occur in electron density at a free electron metal/dielectric interface [37]. It has been widely reported that the wavelength of maximum absorbance (λ_{max}) is dependent on the AgNPs size. In this sense, UV-Vis characterization of nanoparticles obtained by the two different routes were conducted. AgNPs prepared by route A presented an absorbance peak located at 387 nm (not showed in this work). To characterize nanoparticles synthetized by route B, UV-Vis absorbance of the copolyurethane and AgNPs/copolyurethane nanocomposites were acquired (Figure 4.a and 4.b). Pure copolymer exhibited a band at wavelengths of ~ 290 nm. When AgNPs were synthesized directly in the copolyurethane solution, the suspension turns to a stabilized yellowish color after 10 min, compared to the blueish color appeared when the nanoparticles were prepared in absence of the polymer matrix (Figure 4.c). The generation of the nanoparticulate material was corroborated by the additional band positioned at a range of ~ 330 – 335 nm (Figure 4.b), depending on the composite type. J. Sackey et al. [38] observed that, although, generally the plasmon resonance of AgNPs is located at ~ 420 nm, for AgNPs synthesized with the green process using red dye extracts of the *Callistemon viminalis* and an average size of 58.5 nm, it was positioned at 310 nm. An increase of Ag content in the system caused a shift of the maximum absorbance wavelength to lower values (Figure 4.d), indicating the reduction of the AgNPs size. Additionally, an increase in intensity was found as the Ag/copolyurethane ratio increases, which is attributed to a major number of AgNPs formed [39].

To analyze the morphology and particle range size of the AgNPs TEM studies were performed (Figure 5). In the case of the AgNPs synthesized following route A, they presented a mean equivalent diameter 15.8 nm with a standard deviation of 4.5. Furthermore, the confidence interval (lower and upper limits) has been calculated, which means that the proportion of samples of a given size that may be expected to contain the mean value, in our case for the 95 % (Figure 5 and Table 2). These results were in concordance with previously reported works in which the important role of the temperature and the $NaBH_4$ concentration was highlighted in order to control de nanoparticle size [40–42]. However, those synthesized by route B were spherical with main average diameter around three time smaller, 5.6 nm and standard deviation of 2.9 nm (Figure 5 and Table 2).

With all data describing these two approaches to obtain the corresponding AgNPs in hand, it was possible to elucidate the best choice for the coating based on several aspects to accurately assess the relative benefits and risks of using AgNPs. In this sense, these metallic nanoparticles exhibit size-dependent mechanisms of cell uptake that profoundly determine their bioavailability, with a 'Trojan Horse' mechanism, being able to passively penetrate cell walls and membranes to produce higher levels of intracellular Ag^+, causing cytotoxic and genotoxic effects by the disruption of cell transport and local depletion of glutathione and other anti-oxidants when they are smaller or around 5 nm [43,44]. Apart from toxicity related to smaller sizes, there are other reasons to support approach A, such as lower cost compared to a multi-step polymer synthesis or a higher reproducible method that would not require air free techniques with skilled workmanship, as well as a higher metallic nanoparticles concentration in the first approach.

3.3 Microstructural and chemical analyses of the AgNPs coated c.p. Ti substrates

Once both, substrates and AgNPs were characterized, substrate surfaces were silanized with APTES to introduce amino group, which can interact with Ag^0 and improve AgNP adherence to the sample surface. Silanization was carried out by substrate treatment with

piranha solution, a strong oxidizing agent used to hydroxylate (increase the number of -OH groups) sample surfaces. Reaction of hydroxyl groups with APTES lead to the inclussion -NH_2 groups in the Ti substrates. Then, they were coated with the AgNPs synthesized by the selected route. The coating procedure was carried out by immersion in the nanoparticle suspension. Figure 6 displays SEM images of the coated porous c.p. Ti substrates where the homegenous coating can be observed. Details of these images (inset) show some agglomeration of the AgNPs, although they were not frequent.

The surface of the coated substrates was also characterized by compositional analyses technique. As an example, Figure 7a shows an EDS-SEM spectrum of the SEM images (Inset of that panel) as well as the Si distribution on the surface. It could be observed that Si on the whole surface confirms that the silanization process occurred. Other EDS acquired on the AgNPs conglomerated confirmed the presence of AgNPs (Figure 7c). Punctual EDS on the substrate were also carried out (Figure 7b).

3.4 Antibacterial behavior

In previous works, authors have already evaluated the bacterial behavior of porous Ti substrates with different proportions and sizes of pores [4], revealing a greater bacterial adhesion and proliferation in those samples with bigger pore size distribution. Similarly, they investigated a novel methodology to confer antimicrobial character to these Ti substrates by the application of SPEEK coatings [45,46]. On the other hand, various techniques have been applied with silver as the protagonist: thin films of Ag-SiO_2 nanocomposites of the sol gel type, materials of Ag / TiO_2 and AgNPs composites embedded in porous matrices [47,48]. However, a different tandem (AgNPs chemically attached to porous Ti) to evaluate its efficiency is envisaged in the present research work. Therefore, experiments to estimate the efficacy of the chemical bound of AgNPs to Ti and the influence of the pore size in the bacterial inhibition properties of Ti substrates were conducted on silanized (as a control) and

AgNP-coated samples with a 40 % of porosity (Figure 8). These experiments were based on a preliminary qualitative analysis and demonstrated that inhibitory halos appeared in AgNPs-functionalized porous Ti substrates (Figure 8d), while these halos were not observed in silanized Ti samples (Figures 8c). Figure 8b displays the results of the bacterial inhibition for samples of 40% of porosity and both, 100–200 and 355–500 μm, pore size distribution, showing the inhibition diameter compared to the substrate diameter, exhibiting the difference between them, what corresponds to the inhibition halo produced by the diffusion of Ag^+ ions. In both cases, the inhibition halo appeared after samples incubation corresponded to 15 mm that, with the 11.3 mm of sample diameter results in an inhibition halo of slightly inferior to 4 mm. However, if the results are analyzed in detail, we can indicate that the inhibition is slightly higher in the substrates with larger pores. This fact could be attributed to the fact that it is easier to introduce and deposit silver nanoparticles on the walls of this type of pore. The antibacterial role of the surface modification with silver nanos in this type of substrate is much more important in relative terms considering that on virgin substrates with larger pores higher accumulation of bacteria has been reported [4].

4. Conclusions

In summary, porous c.p. titanium substrates are successfully obtained using the spacer-holder technique, in terms of pore content and size. The substrates with smaller pore sizes exhibit better mechanical balance, while those of larger size would allow not only better bone growth towards the interior of the bone but also a more efficient deposition of the silver nanoparticles proposed in this work. Two different routes to obtain AgNPs have been explored. Although the use of copolyurethane is a very suitable additive in terms of stabilization, it has been proved that $NaBH_4$-reduced AgNPs exhibit a better and more convenient biological performance due its particle size. On the other hand, the silanization process used to chemically bond AgNPs to porous c.p. Ti as an appropriate coating was simple, easily reproducible and achieved adequate nanoparticle size to avoid toxicity

compared to the alternative route that uses biodegradable polymers. Preliminary results testing antimicrobial performance of these materials were carried out with *Staphylococcus aureus* to conclude that the AgNP coating process induces antibacterial characteristics to both titanium substrates with 40 vol. % of porosity. However, the fact that previous studies carried out by the authors demonstrated a greater adhesion and proliferation of bacteria in virgin c.p. Ti substrates of largest pore size, highlights a more relevant effectiveness of AgNPs-coated Ti substrates to avoid the bacterial proliferation

Acknowledgments: The authors dedicate this paper to the memory of Juan J. Pavón Palacio (University of Antioquia, Colombia). Also thank to Freiman Segura, Juan Guillermo Castaño and Durley Eliana Restrepo for his support in bacterial tests. This work was supported by the Ministry of Science and Innovation of Spain under the grant PID2019-109371GB-I00, by the Junta de Andalucía–FEDER (Spain) through the Project Ref. US-1259771 and by the Junta de Andalucía-Proyecto de Excelencia (Spain) P18-FR-2038.

References

[1] T.T. Tang, L. Qin, Translational study of orthopaedic biomaterials and devices, J Orthop Transl. 5 (2016) 65-71. https://doi.org/10.1016/j.jot.2016.02.001.
[2] H. Al-Imam, E.B. Özkaya, A.R. Benetti, A.M. Pedersen, K. Gotfredsen, Oral health-related quality of life and complications after treatment with partial removable dental prosthesis, J Oral Rehabil. 43 (2016) 23-30. https://doi.org/10.1111/joor.12338.
[3] Y. Yang, N. Oh, Y. Liu, W. Chen, S. Oh, M. Appleford, S. Kim, K. Kim, S. Park, J. Bumgardner, W. Haggard, J. Ong, Enhancing Osseointegration Using Surface-Modified Titanium Implants, JOM. 58 (2006) 71-76. https://doi.org/10.1007/s11837-006-0146-1.
[4] A. Civantos, A.M. Beltrán, C. Domínguez-Trujillo, M.D. Garvi, J. Lebrato, J.A. Rodríguez-Ortiz, F. García-Moreno, J. V. Cauich-Rodriguez, J.J. Guzman, Y. Torres, Balancing porosity and mechanical properties of titanium samples to favor cellular growth against bacteria, Metals (Basel). 9 (2019). https://doi.org/10.3390/met9101039.
[5] B. Kasemo, Biocompatibility of titanium impants: A Surface science aspects, J. Prosthet. Dent. 49 (1983) 832-837. https://doi.org/10.1016/0022-3913(83)90359-1.
[6] E. Rompen, O. Domken, M. Degidi, A.E. Pontes, A. Piattelli, The effect of material characteristics, of surface topography and of implant components and connections on soft tissue integration: a literature review, Clin Oral Implant. Res. 17 Suppl 2 (2006) 55-67. https://doi.org/10.1111/j.1600-0501.2006.01367.x.
[7] S. Yamano, Al-Sowygh, Z. H., Gallucci, G. O., Wada, Keisuke, Weber, Hans-Peter, Sukotjo, Cortino, Early peri-implant tissue reactions on different titanium surface topographies, Clin. Oral Implants Res. 22 (2010) 815-819. https://doi.org/10.1111/j.1600-0501.2010.02059.x.
[8] J.M. Brown, J.B. Mistry, J.J. Cherian, R.K. Elmallah, M. Chughtai, S.F. Harwin, M.A.

Mont, Femoral Component Revision of Total Hip Arthroplasty, Orthopedics. 39 (2016) e1129-e1139. https://doi.org/10.3928/01477447-20160819-06.
[9] R.O. Darouiche, Treatment of infections associated with surgical implants, N Engl J Med. 350 (2004) 1422-1429. https://doi.org/10.1056/NEJMra035415.
[10] M. Chen, L. Yang, L. Zhang, Y. Han, Z. Lu, G. Qin, E. Zhang, Effect of nano/micro-Ag compound particles on the bio-corrosion, antibacterial properties and cell biocompatibility of Ti-Ag alloys, Mater Sci Eng C Mater Biol Appl. 75 (2017) 906-917. https://doi.org/10.1016/j.msec.2017.02.142.
[11] J. Raphel, M. Holodniy, S.B. Goodman, S.C. Heilshorn, Multifunctional coatings to simultaneously promote osseointegration and prevent infection of orthopaedic implants, Biomaterials. 84 (2016) 301-314. https://doi.org/10.1016/j.biomaterials.2016.01.016.
[12] Y.H. An, R.J. Friedman, Concise review of mechanisms of bacterial adhesion to biomaterial surfaces, J Biomed Mater Res. 43 (1998) 338-348. https://doi.org/10.1002/(sici)1097-4636(199823)43:3<338::aid-jbm16>3.0.co;2-b.
[13] D.E. Moormeier, K.W. Bayles, Staphylococcus aureus biofilm: a complex developmental organism, Mol Microbiol. 104 (2017) 365-376. https://doi.org/10.1111/mmi.13634.
[14] M. Moritz, M. Geszke-Moritz, The newest achievements in synthesis, immobilization and practical applications of antibacterial nanoparticles, Chem. Eng. J. 228 (2013) 596-613. https://doi.org/10.1016/j.cej.2013.05.046.
[15] B. Brusham, Springer Handbook of Nanotechnology, Springer, 2017.
[16] Nanoparticles' Promises and Risks: Characterization, Manipulation, and Potential Hazards to Humanity and the Environment, Springer, 2015.
[17] C. Bankier, R.K. Matharu, Y.K. Cheong, G.G. Ren, E. Cloutman-Green, L. Ciric, Synergistic Antibacterial Effects of Metallic Nanoparticle Combinations, Sci Rep. 9 (2019) 16074. https://doi.org/10.1038/s41598-019-52473-2.
[18] Y. Torres, S. Lascano, J. Bris, J. Pavón, J.A. Rodriguez, Development of porous titanium for biomedical applications: A comparison between loose sintering and space-holder techniques, Mater. Sci. Eng. C. 37 (2014) 148-155. https://doi.org/10.1016/j.msec.2013.11.036.
[19] S. Ferraris, A. Venturello, M. Miola, A. Cochis, L. Rimondini, S. Spriano, Antibacterial and bioactive nanostructured titanium surfacesfor bone integration, Appl. Surf. Sci. 311 (2014) 279-291. https://doi.org/10.1016/j.apsusc.2014.05.056.
[20] M. Khodaei, M. Fathi, M. Meratian, O. Savabi, The effect of porosity on the mechanical properties of porous titanium scaffolds : comparative study on experimental and analytical values, Mater. Res. Express. 5 (2018) 55401. https://doi.org/10.1088/2053-1591/aabfa2.
[21] M. Zahran, A.H. Marei, Innovative natural polymer metal nanocomposites and their antimicrobial activity, Int J Biol Macromol. 136 (2019) 586-596. https://doi.org/10.1016/j.ijbiomac.2019.06.114.
[22] A.J. Lucas, J.L. Sproston, P. Barton, R.J. Riley, Estimating human ADME properties, pharmacokinetic parameters and likely clinical dose in drug discovery, Expert Opin Drug Discov. 14 (2019) 1313-1327. https://doi.org/10.1080/17460441.2019.1660642.
[23] Y. Torres, P. Trueba, J. Pavón, I. Montealegre, J.A. Rodríguez-Ortiz, Designing, processing and characterisation of titanium cylinders with graded porosity: An alternative to stress-shielding solutions, Mater. Des. 63 (2014) 316-324. https://doi.org/10.1016/j.matdes.2014.06.012.
[24] Standard Test Method for ASTM C373-14, Standard Test Method for Water Absorption, Bulk Density, Apparent Porosity, and Apparent Specific Gravity of Fired Whiteware Products, Ceramic Tiles, and Glass Tiles, West Conshohocken, PA, 2014. https://doi.org/10.1520/C0373-14.

[25] P. Trueba, A.M. Beltrán, J.M. Bayo, J.A. Rodríguez-ortiz, D.F. Larios, E. Alonso, D.C. Dunand, Y. Torres, Porous titanium cylinders obtained by the freeze- casting technique: Influence of process parameters on porosity and mechanical behavior, Metals 10 (2020). https://doi.org/10.3390/met10020188.

[26] P.C. Lee, D. Melsel, Adsorption and Surface-Enhanced Raman of Dyes on Silver and Gold Sols, J. Phys. Chem. 86 (1982) 3391-3395. https://doi.org/10.1021/j100214a025.

[27] B. Vlckova, M. Moskovits, I. Pavel, K. Siskova, M. Sladkova, M. Slouf, Single-molecule surface-enhanced Raman spectroscopy froma molecularly-bridged silver nanoparticle dimer, Chem. Phys. Lett. 455 (2008) 131–134. https://doi.org/10.1016/j.cplett.2008.02.078.

[28] I. Pavel, E. McCarney, A. Elkhaled, A. Morrill, K. Plaxco, M. Moskovits, Label-Free SERS Detection of Small Proteins Modified to Act as Bifunctional Linkers, J Phys Chem C Nanomater Interfaces. 112 (2008) 4880-4883. https://doi.org/10.1021/jp710261y.

[29] B. Begines, M.-V. de-Paz, A. Alcudia, J.A. Galbis, Synthesis of reduction sensitive comb-like polyurethanes using click chemistry, J. Polym. Sci. Part A Polym. Chem. 54 (2016). https://doi.org/10.1002/pola.28367.

[30] B. Begines, A. Alcudia, R. Aguilera-Velazquez, G. Martinez, Y. He, R. Wildman, M.J. Sayagues, A. Jimenez-Ruiz, R. Prado-Gotor, Design of highly stabilized nanocomposite inks based on biodegradable polymer-matrix and gold nanoparticles for Inkjet Printing, Sci. Rep. 9 (2019) 1-12. https://doi.org/10.1038/s41598-019-52314-2.

[31] N.G. Bastús, F. Merkoçi, J. Piella, V. Puntes, Synthesis of highly monodisperse citrate-stabilized silver nanoparticles of up to 200 nm: Kinetic control and catalytic properties, Chem. Mater. 26 (2014) 2836-2846. https://doi.org/10.1021/cm500316k.

[32] X. Li, L. Jiang, Q. Zhan, J. Qian, S. He, Localized surface plasmon resonance (LSPR) of polyelectrolyte-functionalized gold-nanoparticles for bio-sensing, Colloids Surfaces A Physicochem. Eng. Asp. 332 (2009) 172-179. https://doi.org/10.1016/j.colsurfa.2008.09.009.

[33] W. Li, X. Xu, W. Li, P. Liu, Y. Zhao, Q. Cen, M. Chen, One-step synthesis of Ag nanoparticles for fabricating highly conductive patterns using infrared sintering, J. Mater. Res. Technol. 9 (2020) 142-151. https://doi.org/10.1016/j.jmrt.2019.10.039.

[34] L. Biao, S. Tan, X. Zhang, J. Gao, Z. Liu, Y. Fu, Synthesis and characterization of proanthocyanidins-functionalized Ag nanoparticles, Colloids Surfaces B Biointerfaces. 169 (2018) 438-443. https://doi.org/10.1016/j.colsurfb.2018.05.050.

[35] A. Franconetti, J.M. Carnerero, R. Prado-Gotor, F. Cabrera-Escribano, C. Jaime, Chitosan as a capping agent: Insights on the stabilization of gold nanoparticles, Carbohydr. Polym. 207 (2019) 806-814. https://doi.org/https://doi.org/10.1016/j.carbpol.2018.12.046.

[36] T.J. Jayeoye, O.O. Olatunde, S. Benjakul, T. Rujiralai, Synthesis and characterization of novel poly(3-aminophenyl boronic acid-co-vinyl alcohol) nanocomposite polymer stabilized silver nanoparticles with antibacterial and antioxidant applications, Colloids Surfaces B Biointerfaces. 193 (2020) 111112. https://doi.org/https://doi.org/10.1016/j.colsurfb.2020.111112.

[37] E. Bulut, M. Özacar, Rapid, facile synthesis of silver nanostructure using hydrolyzable tannin, Ind. Eng. Chem. Res. 48 (2009) 5686-5690. https://doi.org/10.1021/ie801779f.

[38] J. Sackey, A. Fell, J.B. Ngilirabanga, L.C. Razanamahandry, S.K.O. Ntwampe, M. Nkosi, Materials Today : Proceedings Antibacterial effect of silver nanoparticles synthesised on a polycarbonate membrane, Mater. Today Proc. (2020). https://doi.org/10.1016/j.matpr.2020.04.121.

[39] A.R. Lokanathan, K.M.A. Uddin, O.J. Rojas, J. Laine, Cellulose nanocrystal-mediated synthesis of silver nanoparticles: Role of sulfate groups in nucleation phenomena, Biomacromolecules. 15 (2014) 373-379. https://doi.org/10.1021/bm401613h.

[40] M.A. Hegazy, E. Borham, Preparation and characterization of silver nanoparticles homogenous thinfilms, NRIAG J. Astron. Geophys. 7 (2018) 27-30. https://doi.org/10.1016/j.nrjag.2018.04.002.
[41] S.U. Nur, P. Anung, L. Enny, S. Endang, L. Hotman, W. Triani, F. Siska, Critical Parameters of Silver Nanoparticles (AgNPs) synthesized by Sodium Borohydride Reduction, Res. J. Chem. Environ. 22 (2018) 179-183.
[42] S. Agnihotri, S. Mukherji, S. Mukherji, Size-controlled silver nanoparticles synthesized over the range 5–100 nm using the same protocol and their antibacterial efficacy, RSC Adv. 4 (2014) 3974-3983. https://doi.org/10.1039/C3RA44507K.
[43] S.M. Hussain, K.L. Hess, J.M. Gearhart, K.T. Geiss, J.J. Schlager, In vitro toxicity of nanoparticles in BRL 3A rat liver cells, Toxicol Vitr. 19 (2005) 975-983. https://doi.org/10.1016/j.tiv.2005.06.034.
[44] T. Suzuki, Y. Guo, S. Inoue, X. Zhao, M. Ohkohchi, Y. Ando, Multiwalled carbon nanotubes mass-produced by dc arc discharge in He–H2 gas mixture, J. Nanoparticle Res. 8 (2006) 279–285. https://doi.org/10.1007/s11051-005-9004-2.
[45] C. Domínguez-Trujillo, A.M. Beltrán, M.D. Garvi, A. Salazar-Moya, J. Lebrato, D.J. Hickey, J.A. Rodríguez-Ortiz, P.H. Kamm, C. Lebrato, F. García-Moreno, T.J. Webster, Y. Torres, Bacterial behavior on coated porous titanium substrates for biomedical applications, Surf. Coatings Technol. 357 (2019) 896-902. https://doi.org/10.1016/j.surfcoat.2018.10.098.
[46] A.M. Beltrán, A. Civantos, C. Dominguez-Trujillo, R. Moriche, J.A. Rodríguez-Ortiz, F. García-Moreno, T.J. Webster, P.H. Kamm, A.M. Restrepo, Y. Torres, Porous titanium surfaces to control bacteria growth: Mechanical properties and sulfonated polyetheretherketone coatings as antibiofouling approaches, Metals 9 (2019). https://doi.org/10.3390/met9090985.
[47] V.K. Sharma, R.A. Yngard, Y. Lin, Silver nanoparticles: green synthesis and their antimicrobial activities, Adv Colloid Interface Sci. 145 (2009) 83-96. https://doi.org/10.1016/j.cis.2008.09.002.
[48] N. Niño-Martínez, G.A. Martínez-Castañón, A. Aragón-Piña, F. Martínez-Gutierrez, J.R. Martínez-Mendoza, F. Ruiz, Characterization of silver nanoparticles synthesized on titanium dioxide fine particles, Nanotechnology. 19 (2008) 65711. https://doi.org/10.1088/0957-4484/19/6/065711.

Table 1. Porosity and mechanical characterization of porous c.p. Ti substrates.

			Microstructural characterization			Estimated mechanical behavior	
Technique		Pores size	P_T (%)	P_i (%)	D_{eq} (μm)	E_d (GPa)	σ_y (MPa)
Conventional powder metallurgy		Fully-dense	2.4 ± 0.3	1.3 ± 0.3	4.6 ± 2.5	96.2 ± 1.0	580 ± 3
Spacer-holder	40 vol. %	100 – 200 μm	40.2 ± 1.0	32.9 ± 0.7	226 ± 178	45.9 ± 1.1	190 ± 7
		355 – 500 μm	40.8 ± 1.3	27.8 ± 0.9	359 ± 223	45.3 ± 0.8	135 ± 5

Table 2. AgNPs size distribution

	Mean particle diameter (nm)	st. dev. (mean particle, nm)	Minimum (nm)	Maximum (nm)	Confidence interval of the mean (95 %)
Route A	15.8	4.5	9.2	30.2	(14.1, 17.5)
Route B	5.6	2.9	2.0	21.8	(4.9, 6.3)

Figures captions:

Figure 1. Workflow conducted in this investigation.

Figure 2. Schematic of the sugar-based copolyurethane composition.

Figure 3. Polymer assembly for AgNPs stabilization.

Figure 4. UV-vis spectra of synthesized AgNPs/copolyuretane systems: (**a**) full range; (**b**) AgNPs maximum absorbance; (**c**) dependence of AgNs maximum absorbance on concentration; (**d**) suspensions of AgNPs without and with the copolyurethane.

Figure 5. Comparison on the two routes for the synthesis of AgNPs. TEM images, histograms of the AgNPs distribution. HRTEM images corresponds to route B. Note: dark contrast of the TEM image of route A were due to the carbon grid.

Figure 6. 40 vol. % c.p. Ti porous substrates coated by the AgNPs synthetized by route A. Inset: details of the coating.

Figure 7. EDS-SEM of the coated substrates. a) Si-map, b) Punctual EDS-SEM on the substrate and c) punctual EDS-SEM on an AgNPs conglomerate.

Figure 8. Inhibition experiments using substrate of 40% of porosity: measurements criteria (a), general results (b), images for 355-500 um after silanization and before AgNP coating (c) and after AgNP coating (d). Same scale bar for image c) and d)

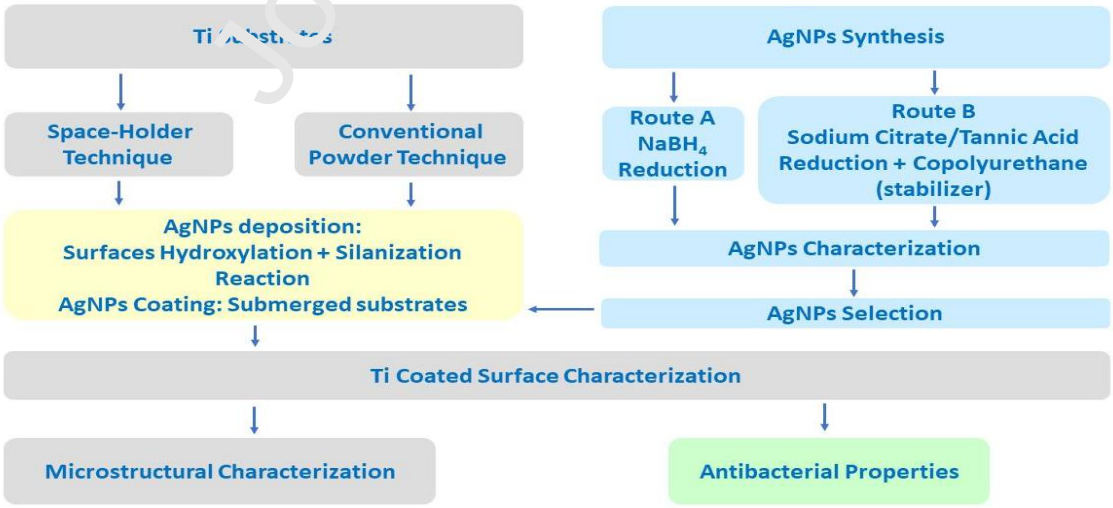

Figure 1

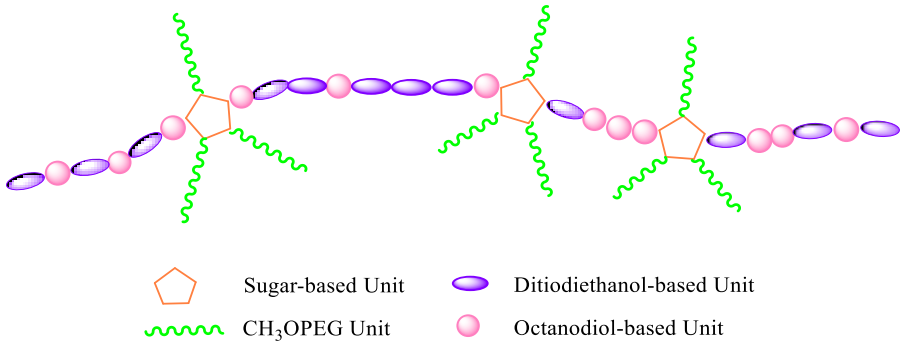

Figure 2

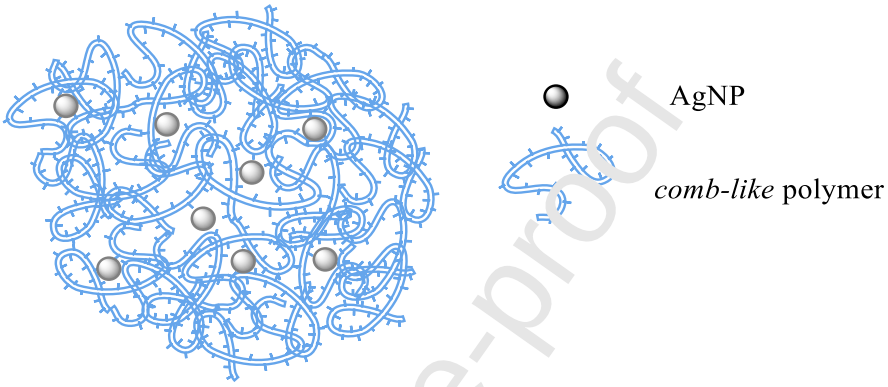

Figure 3

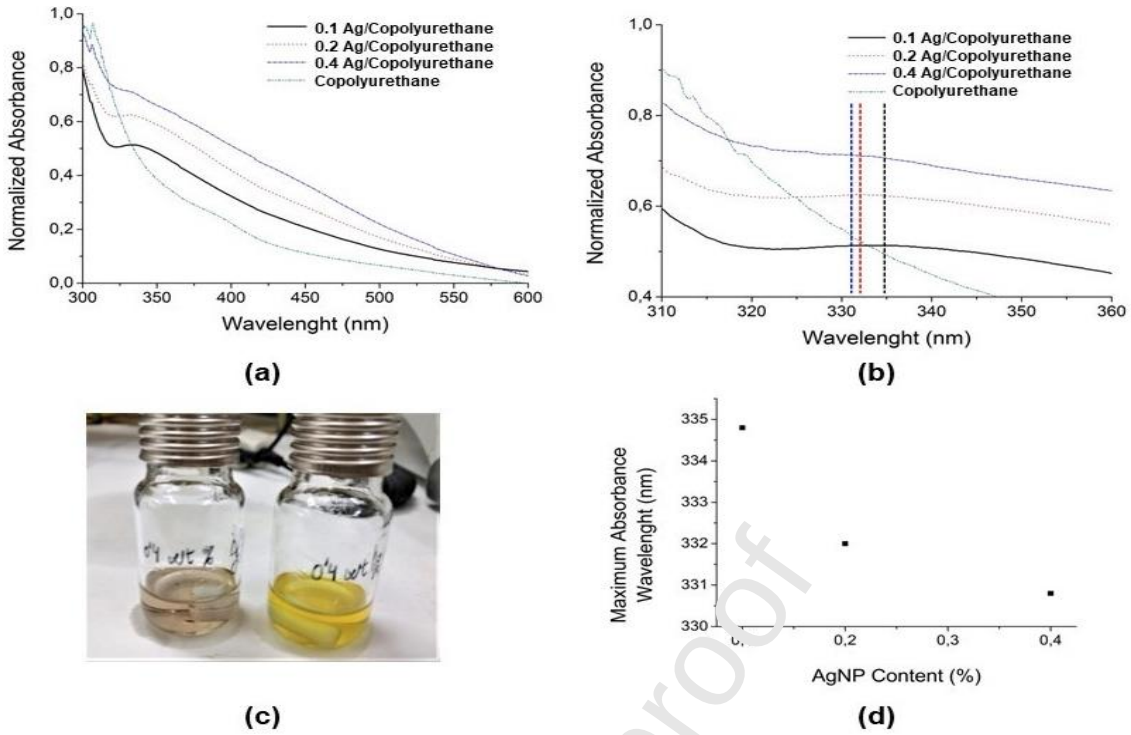

Figure 4

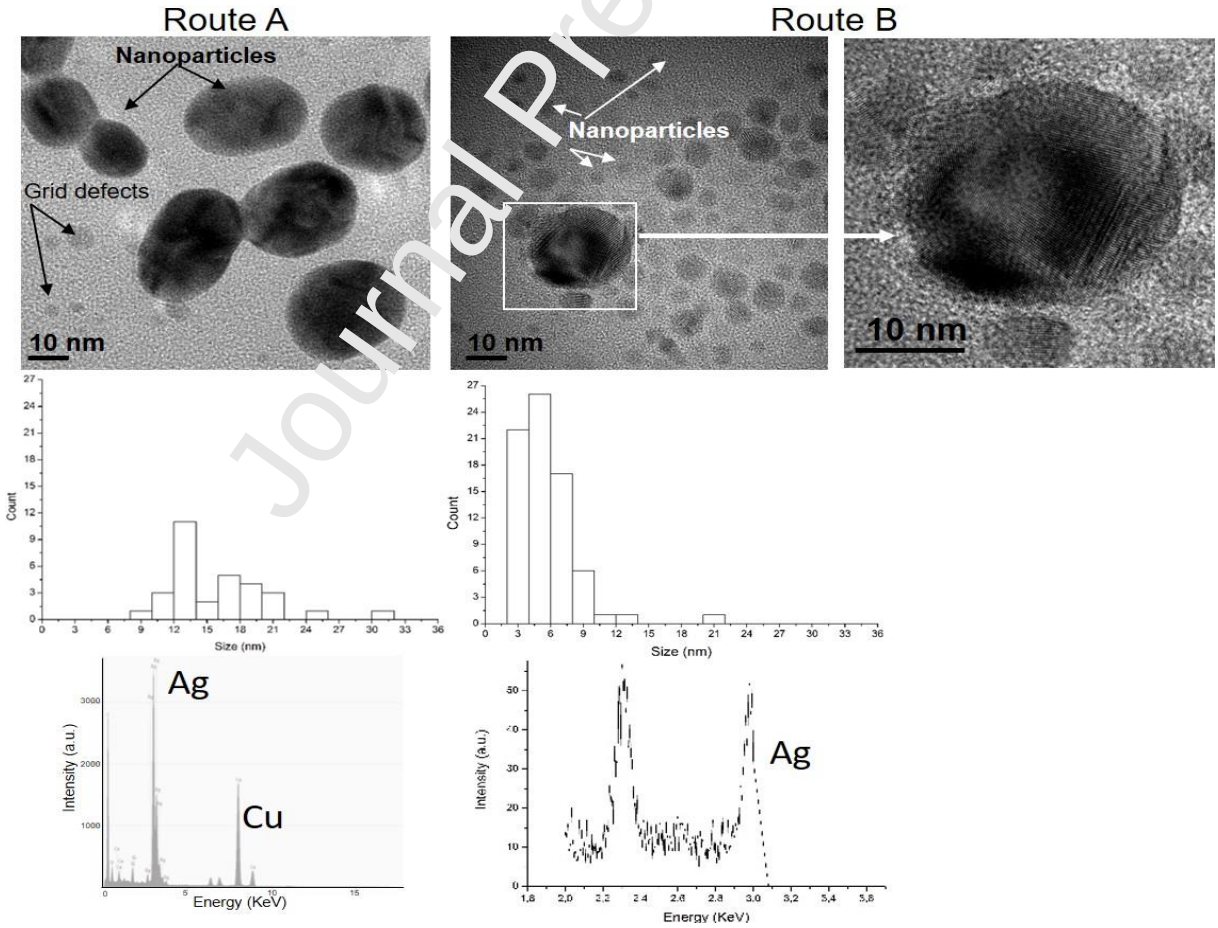

Figure 5

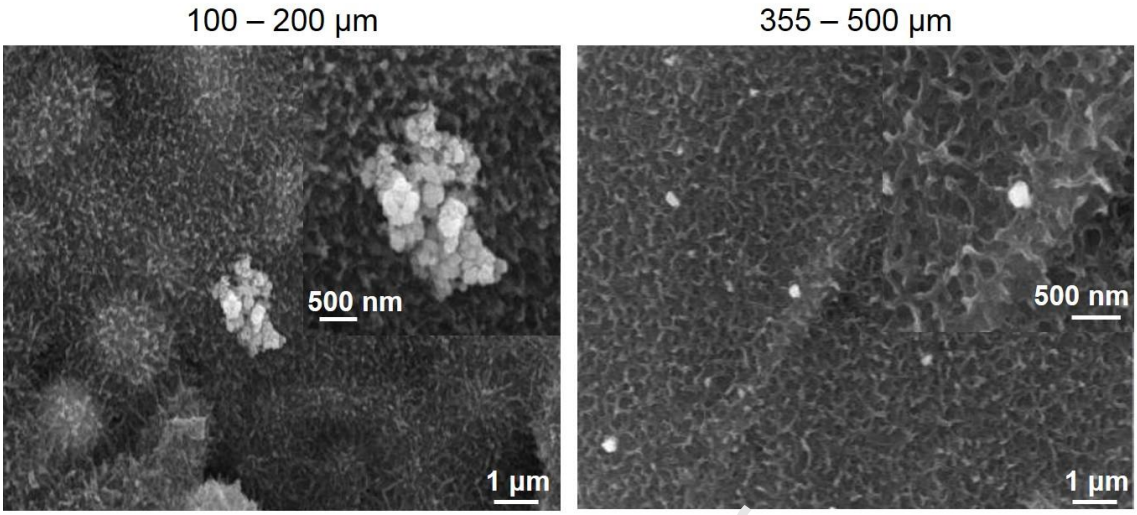

Figure 6

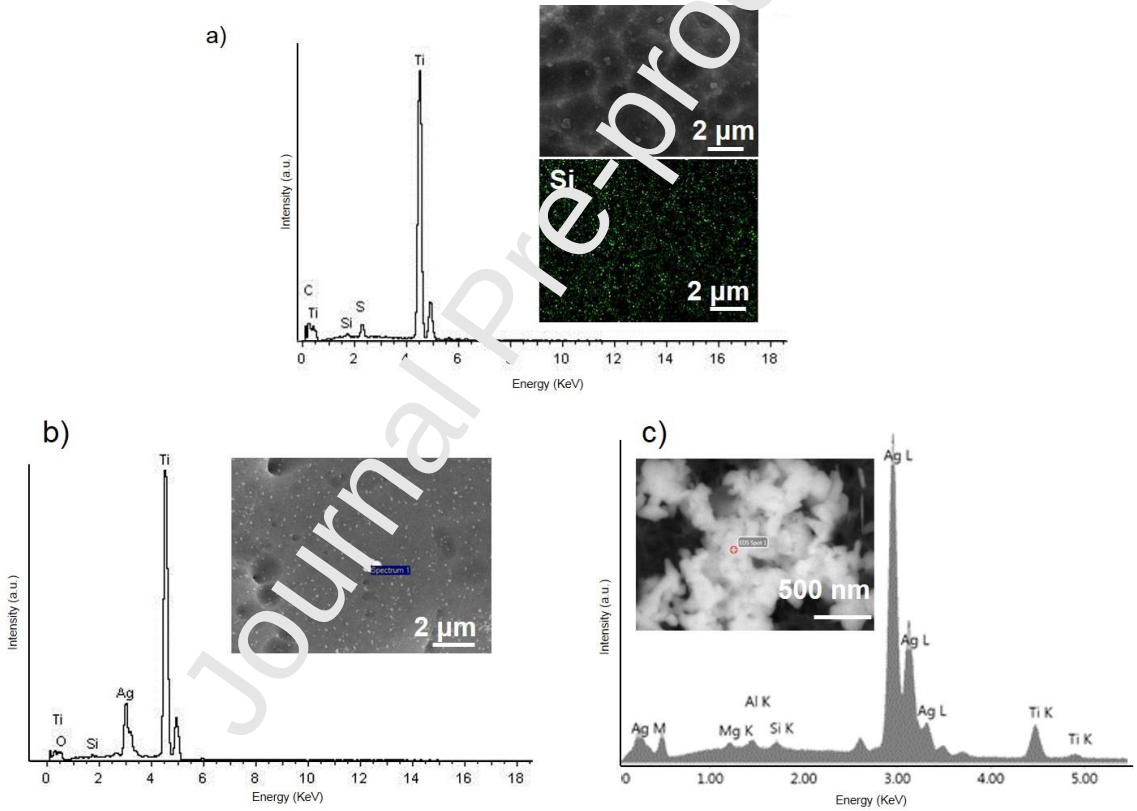

Figure 7

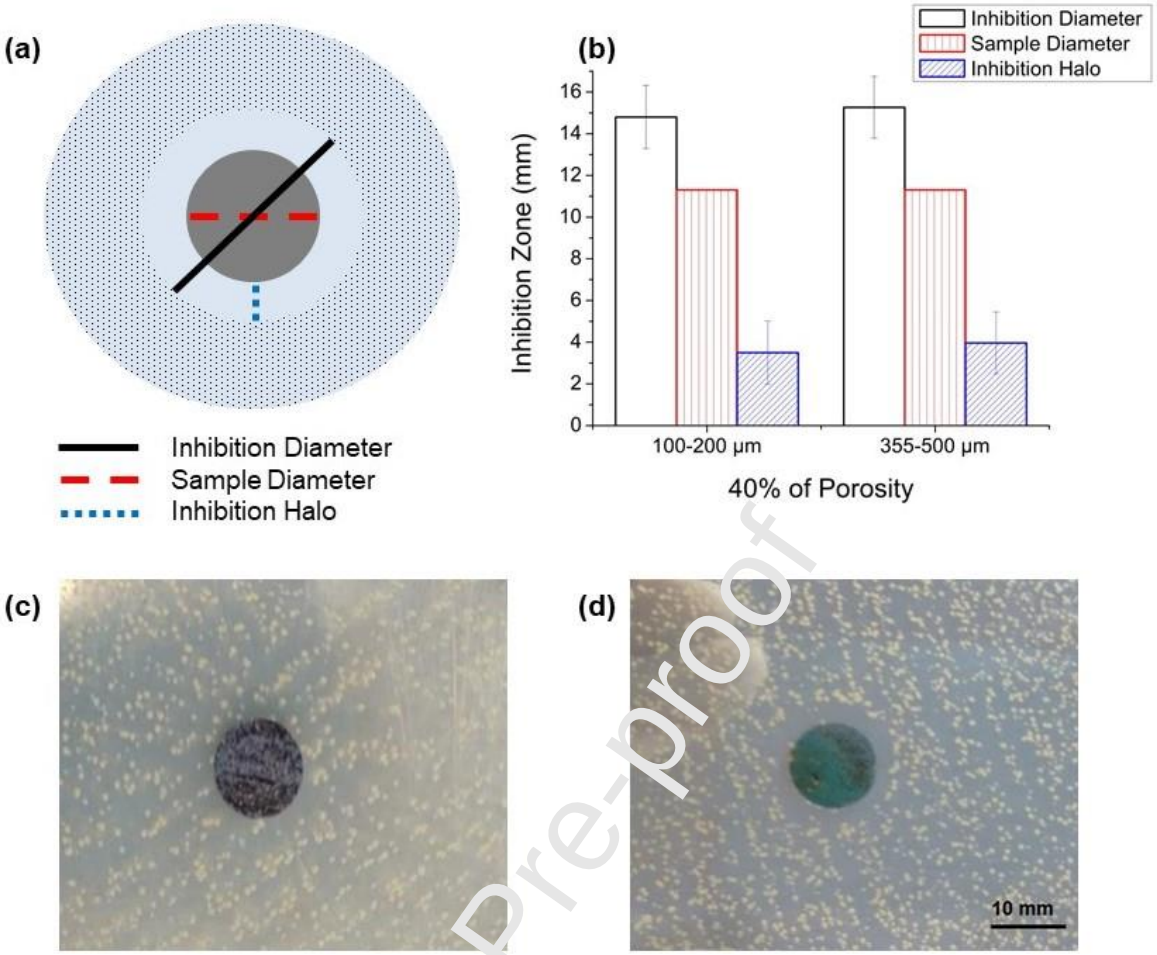

Figure 8

Declaration of competing interests

☒ The authors declare that they have no known competing financial interests or personal relationships that could have appeared to influence the work reported in this paper.

☐The authors declare the following financial interests/personal relationships which may be considered as potential competing interests:

Credits authors statements:

- Conceptualization, project administration, supervision, methodology: J.A.R.O., J.V. and Y.T.
- Investigation, formal analysis, validation: J.G., A.A., B.B., A.M.B. and R.M
- Discussion and writing—original draft preparation, all the authors.

Highlights:

- Synthesis of AgNPs via $NaBH_4$-reduction
- Synthesis of AgNP-polymer nanocomposite using citrate reduction
- Deposition of AgNPs on the surface of titanium substrate after its silanization
- The AgNP coating process induces potential antibacterial characteristics
- Larger pore sizes would allow a more efficient deposition of Ag-NPs

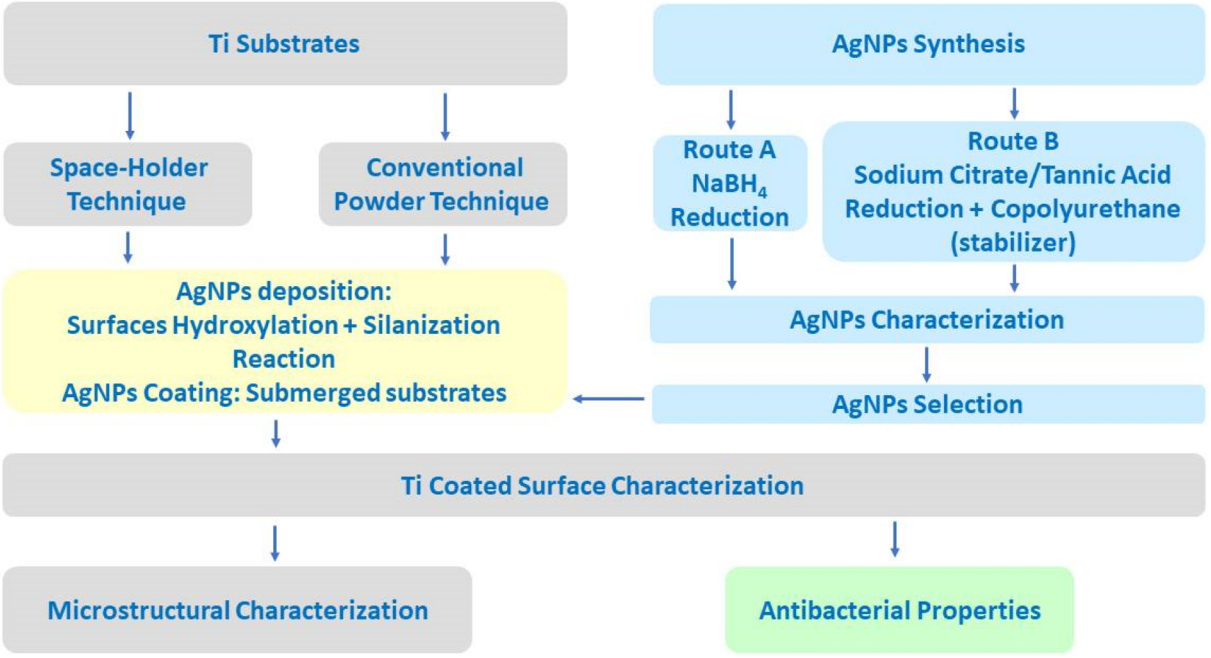
Ti Substrates
AgNPs Synthesis
Space-Holder Technique
Conventional Powder Technique
Route A
NaBH4 Reduction
Route B
Sodium Citrate/Tannic Acid Reduction + Copolyurethane (stabilizer)
AgNPs deposition:
Surfaces Hydroxylation + Silanization Reaction
AgNPs Coating: Submerged substrates
AgNPs Characterization
AgNPs Selection
Ti Coated Surface Characterization
Microstructural Characterization
Antibacterial Properties

Figure 1

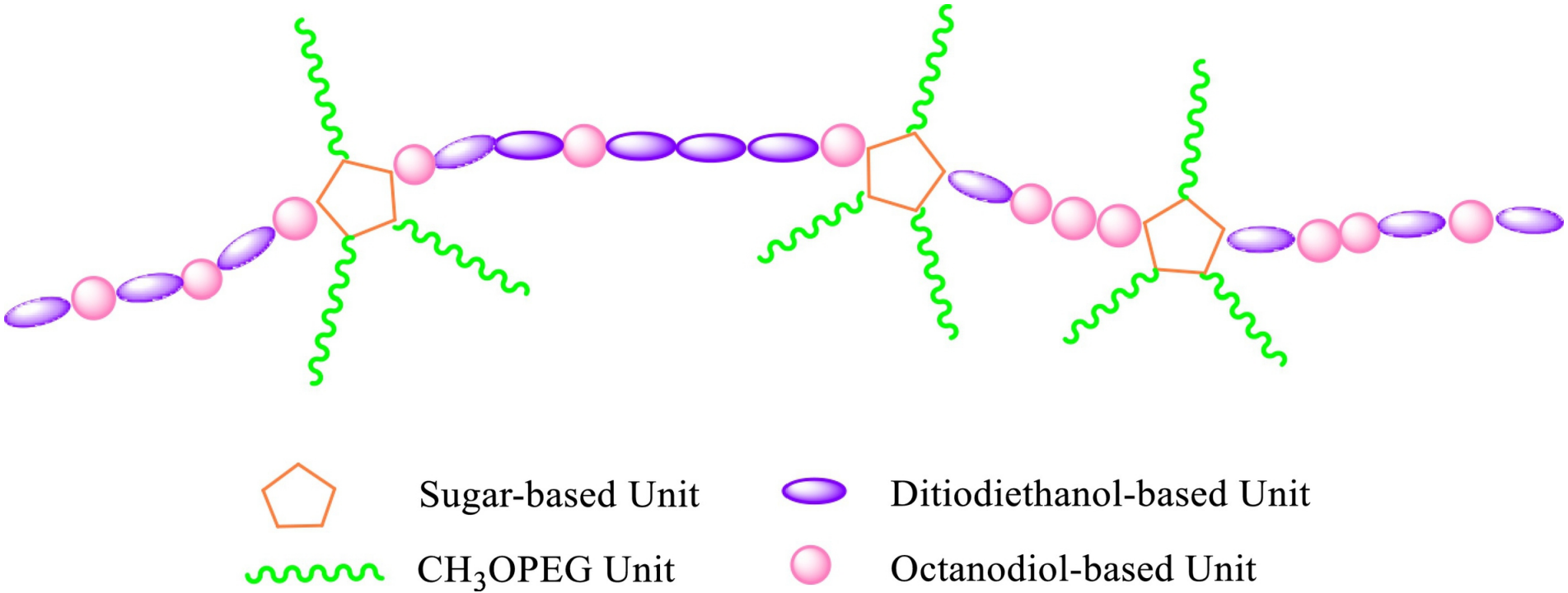
Sugar-based Unit
Ditiodiethanol-based Unit
CH3OPEG Unit
Octanodiol-based Unit

Figure 2

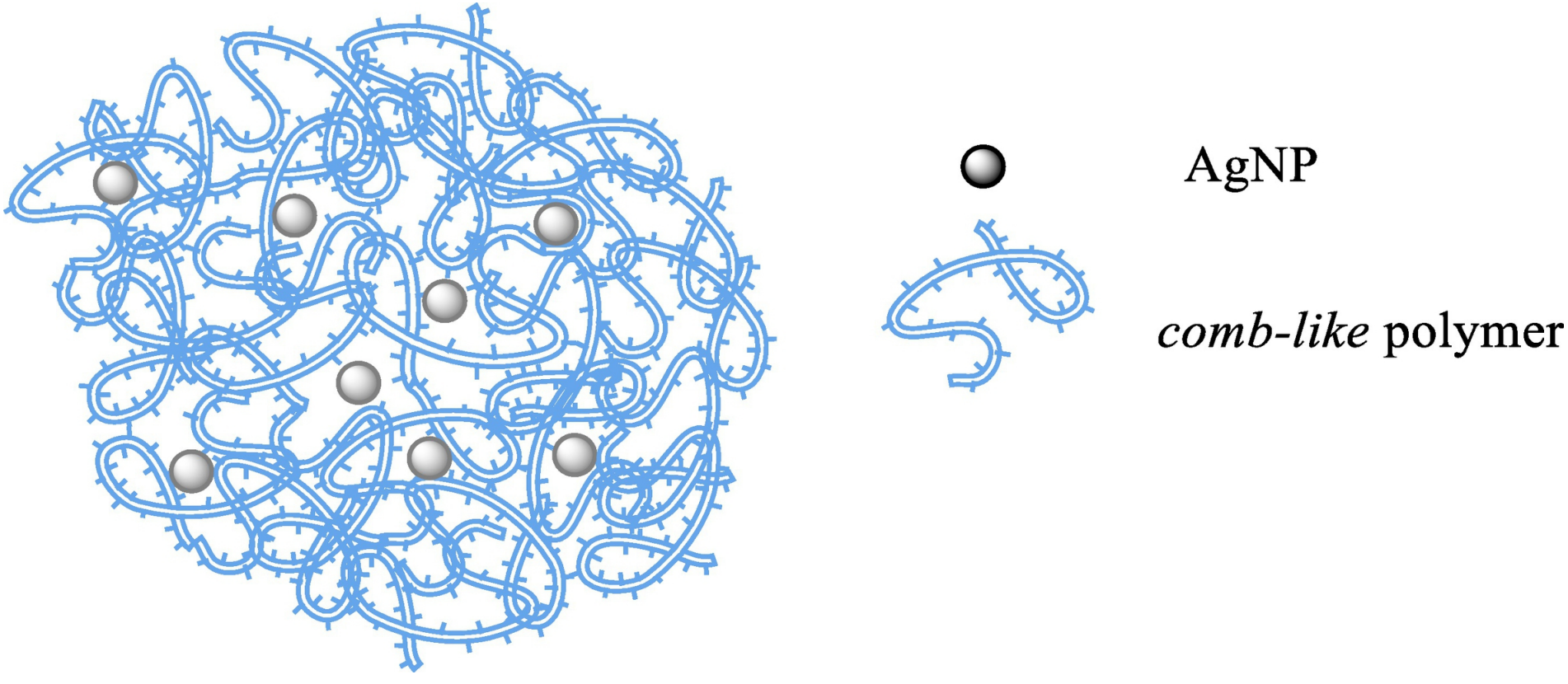

Figure 3

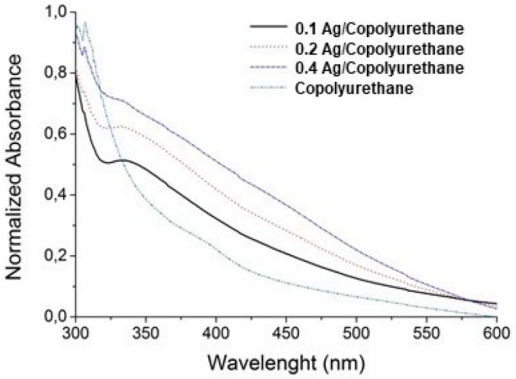

(a)

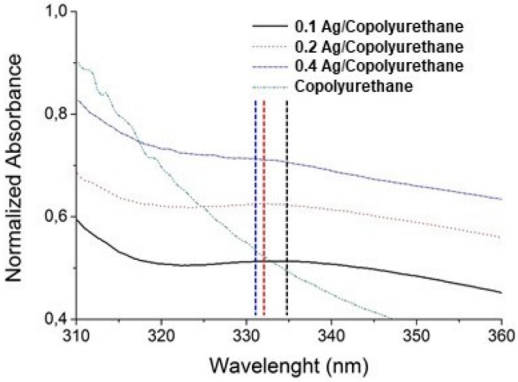

(b)

(c)

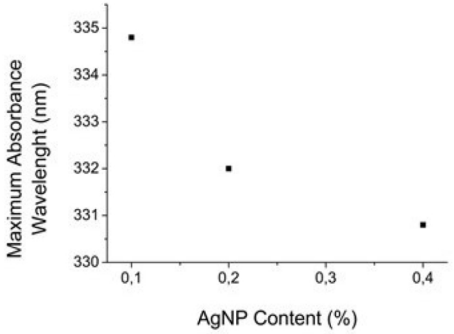

(d)

Figure 4

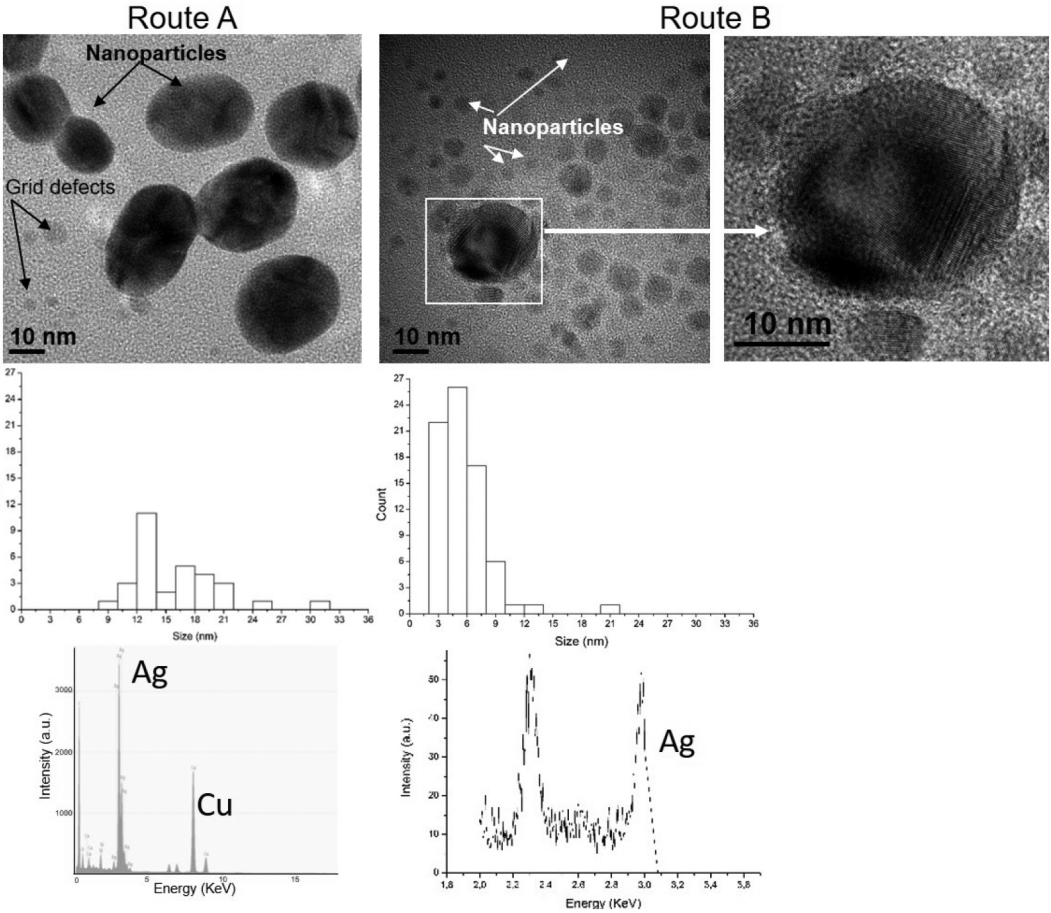
Route A
Route B
Nanoparticles
Grid defects
10 nm
Nanoparticles
10 nm
10 nm
Count
Size (nm)
Count
Size (nm)
Ag
Cu
Intensity (a.u.)
Energy (KeV)
Ag
Intensity (a.u.)
Energy (KeV)

Figure 5

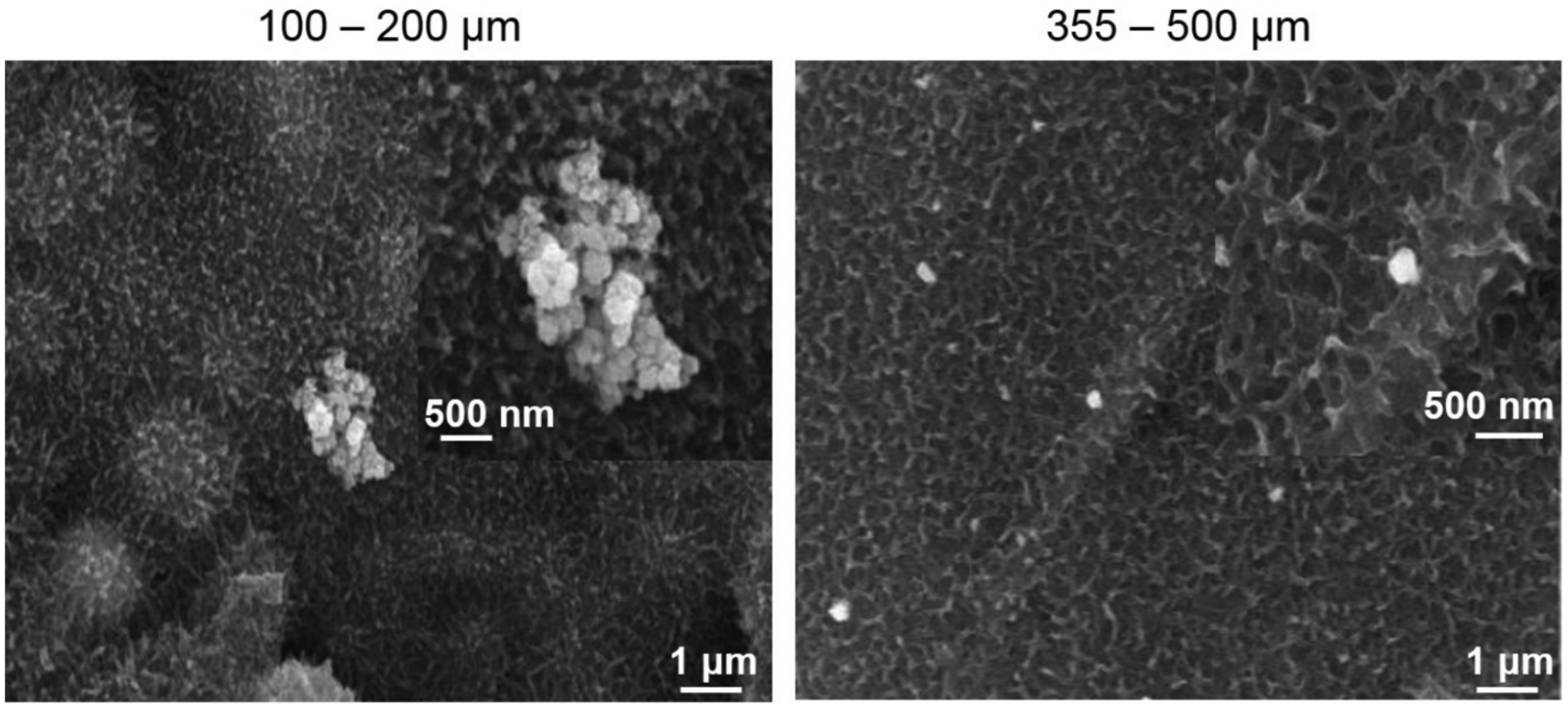

Figure 6

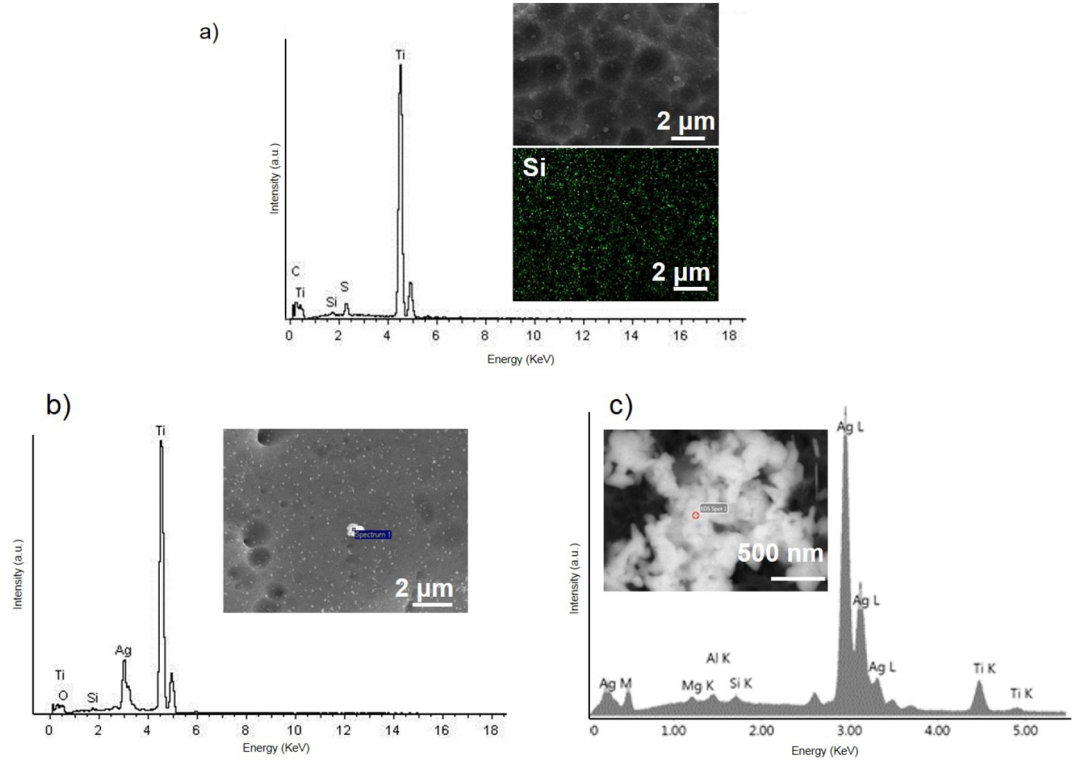
a)
Ti
C
Ti
Si
S
Intensity (a.u.)
0
2
4
6
8
10
12
14
16
18
Energy (KeV)
2 µm
Si
2 µm
b)
Ti
Ag
Ti
O
Si
Intensity (a.u.)
Spectrum 1
2 µm
0
2
4
6
8
10
12
14
16
18
Energy (KeV)
c)
Ag L
500 nm
Ag L
Ag L
Al K
Ag M
Mg K
Si K
Ti K
Ti K
Intensity (a.u.)
0
1.00
2.00
3.00
4.00
5.00
Energy (KeV)

Figure 7

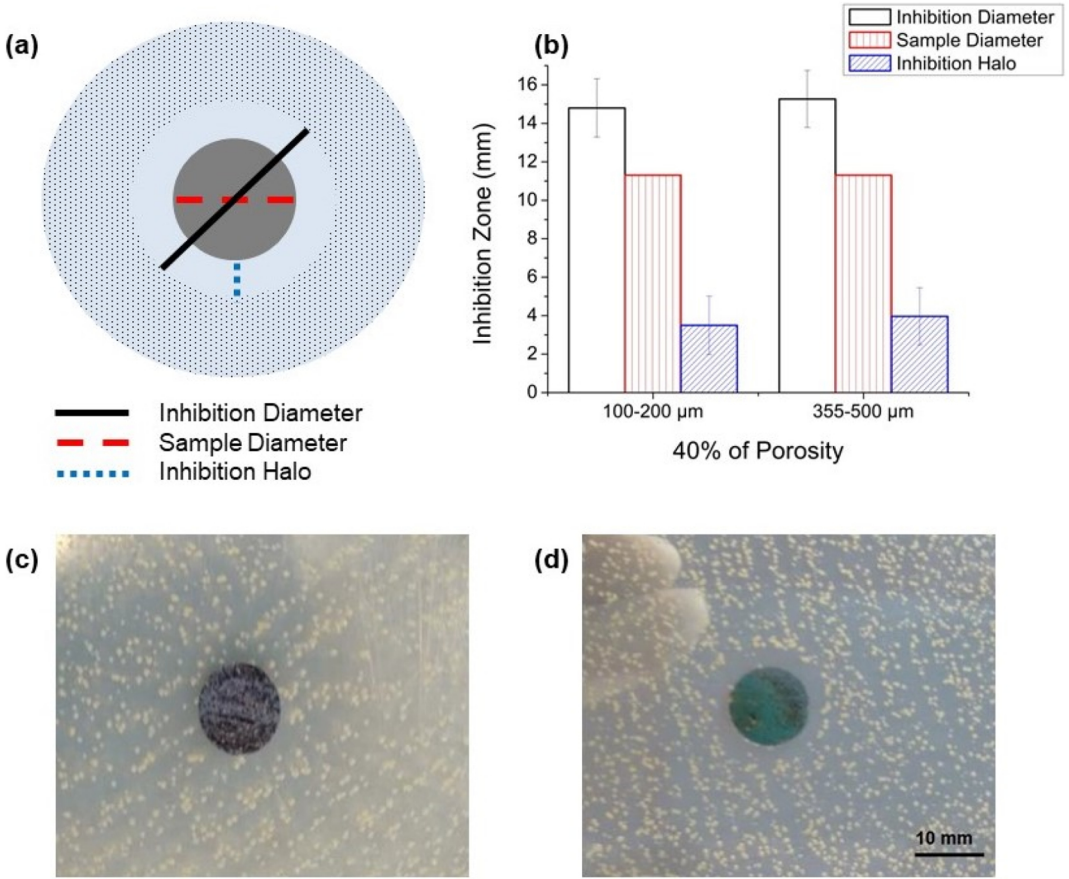
(a)
Inhibition Diameter
Sample Diameter
Inhibition Halo
(b)
Inhibition Diameter
Sample Diameter
Inhibition Halo
Inhibition Zone (mm)
0
2
4
6
8
10
12
14
16
100-200 µm
355-500 µm
40% of Porosity
(c)
(d)
10 mm

Figure 8